DOI: 10.17344/acsi.2020.5963 *Acta Chim. Slov.* **2020,** *67,* 1124–1138

Scientific paper

GO/PAMAM as a High Capacity Adsorbent for Removal of Alizarin Red S: Selective Separation of Dyes

Mohammad Rafi,[1] Babak Samiey[1,*] and Chil-Hung Cheng[2]

[1] *Department of Chemistry, Faculty of Science, Lorestan University, Khoramabad 68137–17133, Lorestan, Iran*

[2] *Department of Chemical Engineering, Ryerson University, M5B 2K3, Toronto, Ontario, Canada*

* *Corresponding author: E-mail: babsamiey@yahoo.com , samiey.b@lu.ac.ir*

Received: 03-16-2020

Abstract

Adsorption of Alizarin Red S (ARS) on graphene oxide/poly(amidoamine) (GO/PAMAM) was studied at different ARS initial concentrations, temperatures, pHs, shaking rates and contact times. Adsorption sites of GO/PAMAM were phenolic –*OH* (*Ph*) group of GO and amine groups (–NH_2, –NH^+_3 and –NHR^+_2) of PAMAM dendrimer moieties of GO/PAMAM. At pH = 2 and 318 K, maximum adsorption capacity ($q_{e,max}$) of the adsorbent was 1275.2 mg g^{-1} which is one of the highest capacity in the literature. Thus, GO/PAMAM in this work acted as a superadsorbent for ARS. At the incipient of adsorption, ARS^- molecules were adsorbed on *Ph* sites that was reaction-controlled step, (E_a = 114.5 kJ mol^{-1}). Adsorption of ARS^-on the remaining sites was diffusion–controlled. In alkaline media, two other types of ARS molecules were identified during that were adsorbed on *Ph* and –NH^+_3 sites. Further increasing the pH of the solution, decreased the number these two sites and yielded a reduced adsorption capacity ($q_{e,max}$). Methylene blue (MB), thionine (Th), pyronin Y (PY), acridine orange (AO), methyl blue (MEB) and janus green (JG) dyes were selectively separated from their mixtures with ARS molecules using GO/PAMAM at pH of 2. The used adsorbent was recycled efficiently by using ethylenediamine very fast.

Keywords Alizarin Red S; GO/PAMAM; Adsorption; ARIAN model; KASRA model; ISO equation

1. Introduction

Wastewater generated by different industries contains pollutant compounds that are hazardous to the health of human beings and animals. Dye compounds included in these pollutants of wastewater are produced by industries like food, paper, rubber, textile, printing, tanning, dyestuff and pigment industries. During the last decades extensive progress has been made for treatment of industrial wastewaters. A number of techniques used for this purpose are filtration,[1] chemical oxidation,[2] ion exchange,[3] biological degradation,[4] reverse osmosis,[5] coagulation,[6] and adsorption.[7] Adsorption is a facile, cost effective and widely-applied method to remove dye compounds from wastewater systems and in many cases can be recycled easily.

Alizarin Red S (ARS), sodium 3,4-dihydroxy-9,10-dioxo-9,10-dihydroanthracene-2-sulfonate, is also known as Mordant Red 3 or Alizarin Carmine which is an anthraquinone and anionic dye. ARS is applied as an acid-base indicator,[8] a red textile dye,[9] for staining in histology[10] and as a chromogenic agent for selective spectroscopic determination of some compounds.[11]

For removing ARS from wastewaters, various kinds of adsorbents were used, such as activated carbon/γ-Fe_2O_3 nano-composite,[12] modified nano-sized silica,[13] magnetic chitosan,[14] *lantana camara*,[15] coconut shell activated carbon,[16] activated clay modified by iron oxide,[17] Fe_3O_4/CeO_2 nanocomposite,[18] calcined [Mg/Al, Zn/Al and MgZn/Al]-LDH,[19] nanocrystalline $Cu_{0.5}Zn_{0.5}Ce_3O_5$,[20] activated carbon engrafted with Ag nanoparticles,[21] nano-Fe_3O_4 and corn cover composite[22] and chitosan/ZnO nanorod composite.[23] The $q_{e,max}$ value values of these adsorbents are tabulated in Table 1.

In this study, graphene oxide/poly(amidoamine) (GO/PAMAM) was synthesized by grafting poly(amidoamine) (PAMAM) dendrimer to graphene oxide.[24–26]

The as-synthesized GO/PAMAM and ARS–adsorbed GO/PAMAM were characterized by different techniques like BET (Brunauer-Emmett-Teller), SEM (Scanning Electron Microscope), EDS (Energy Dispersive X-Ray Spectroscopy), XRD (X-Ray Diffraction) and FTIR

Table 1. Maximum adsorption capacity ($q_{e,max}$) of ARS on a series of adsorbents.

Adsorbent	T (K)	$q_{e,max}$ (mg g^{-1})	Ref.
Activated carbon/γ-Fe2O3	298	108.7	12
Modified nano-sized silica	293	200.0	13
Magnetic chitosan	303	40.1	14
Activated clay modified by iron oxide	298	32.7	17
Fe_3O_4/CeO_2 nanocomposite	303	90.5	18
Activated carbon engrafted with Ag nanoparticles	298	232.6	21
Nano-Fe_3O_4 and corn cover composite	298	10.4	22
GO/PAMAM	328	1275.2	This work

(Fourier Transform Infrared Spectroscopy) techniques. The adsorption process of ARS on GO/PAMAM surface was carried out under different experimental conditions including ARS concentration, ionic strength, pH, temperature, shaking rate and contact time. Due to high adsorption capacity of GO/PAMAM for ARS, GO/PAMAM was considered as a superadsorbent for ARS dye, Table 1.

Kinetics and thermodynamics of adsorption of ARS on GO/PAMAM surface were investigated using the ARIAN and KASRA models respectively that elucidated the process mechanism. Also, high capacity adsorption of GO/PAMAM in acidic pHs for ARS was used for selective separation of a number of dyes from their mixtures with ARS.

2 Experimental

2. 1. Chemicals

Alizarin Red S, alizarin, methylene blue, acridine orange, thionine, pyronin Y, methyl blue, janus green B, sodium hydroxide, sodium chloride, sodium nitrate, potassium permanganate, concentrated sulfuric acid (98%), hydrochloric acid (37%), hydrogen peroxide (30%), methanol (≥99.9%), ethanol (≥99.9%), ethylenediamine (≥99%), diethylenetriamine (≥98%), methyl acrylate (≥99%), *N,N*-dimethylformamide (DMF) (≥99.8%), tetrahydrofuran (THF) (≥99%), acetone (99.8 %), benzene (>99%), dimethylsulfoxide (DMSO) (≥99.9%) and diethyl ether (≥99.7%) were purchased from Merck. Graphite powder (<20 μm) (≥99.9%) was purchased from Sigma-Aldrich. All chemicals were used without further purification.

2. 2. Synthesis of GO/PAMAM

Generation 2 PAMAM (G2 PAMAM) dendrimer (the first generation in this kind of nomenclature is called G–0.5), graphene oxide (GO) and GO/PAMAM were synthesized based on the published procedure.[26]

2. 3. Characterization of GO/PAMAM

The nitrogen-based BET specific surface area of GO/PAMAM was determined by a Pore Size Micrometrics-tristar 3020 instrument, Figure S1. The obtained BET isotherm for GO/PAMAM was type IV and its BET surface area, maximum pore volume (slit pore geometry), adsorption average pore diameter (by BET) and pore volume were 9.59 m^2 g^{-1}, 0.0044 cm^3 g^{-1}, 18.9 nm and 0.045 cm^3 g^{-1}, respectively. It is noticeable that BET surface and pore volume of GO/PAMAM in this work are several times higher than those of reported.[26] Also, its hysteresis loop was H3 which in this case aggregates of platelike GO/PAMAM nanoparticles form slit-like pores.[27]

Scanning electron micrographs (SEM) of GO/PAMAM and ARS-adsorbed GO/PAMAM samples at pHs of 0, 2 and 13 were taken using a MIRA3 TESCAN equipment at 15 keV. The SEM photos of pristine GO/PAMAM and its samples obtained under different conditions exhibited similar surface morphology which were aggregations of PAMAM-covered particles with a porous morphology, Figures 1(a)–1(h). The average size of GO/PAMAM particles estimated by SEM technique was about 30 nm, Figure S2.

EDS spectrum of the as-synthesized GO/PAMAM was acquired by a MIRA3 TESCAN equipment. According to the results of EDS, the atomic percentages of elements on its surface were similar to the published results[26] which confirmed the formation of GO/PAMAM, Figure S3. The XRD pattern of as-synthesized GO/PAMAM was recorded by a Rigaku D-max C III, X-ray diffractometer using Ni-filtered Cu-Kα radiation (λ = 1.5406 Å). The smooth intensity with broad peaks at around 2θ of 26.7° showed that the main structure of GO/PAMAM was amorphous, Figure 2(a). The XRD spectrum of GO/PAMAM was similar to that in the literature.[26]

Also, the FTIR spectrum of GO/PAMAM was taken by a Nicolet IR 100 (Thermo Scientific) FTIR spectrophotometer using KBr pellet technique, Figure 3(a). The peak at 1185 cm^{-1} was assigned to the stretching vibration of C–OH (phenolic) groups of GO/PAMAM.[26,28,29] The spectrum was very similar to that of the previous report for GO/PAMAM.[26] The absence of the peak at 1680–1760 cm^{-1} confirmed the lack of carboxylic acid group in GO/PAMAM. Diminishing the C=O band of GO at 1731cm^{-1} and the appearance bands at 1637 cm^{-1} (C=O amide I stretching vibration mode),[24,29,30] in the IR spectrum of as-synthesized GO/PAMAM confirmed that the GO/PAMAM was synthesized.

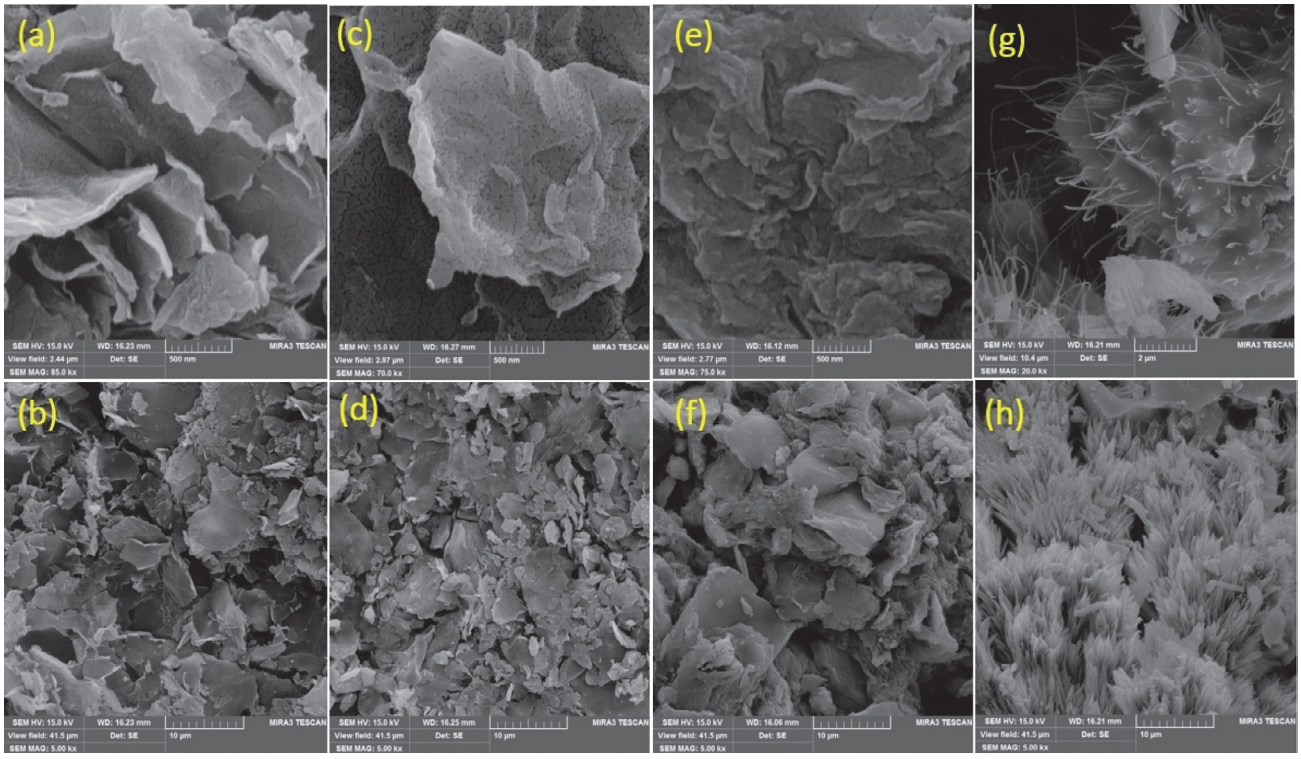

Figure 1. SEM images of (a,b) pristine GO/PAMAM, (c,d) GO/PAMAM modified at pH = 0 and ARS-adsorbed GO/PAMAM samples at (e,f) pH = 2 and (g,h) pH = 13.

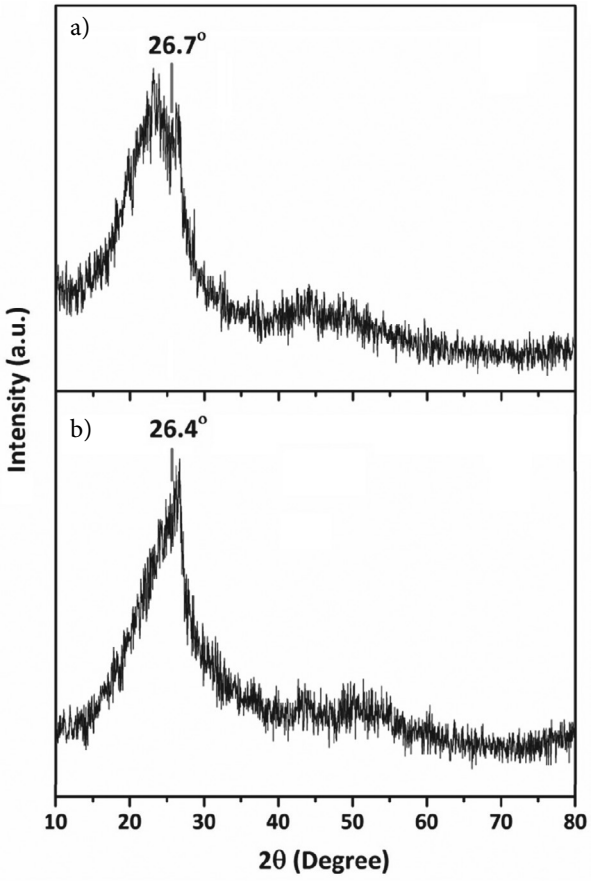

Figure 2. XRD spectra of (a) pristine GO/PAMAM, (b) GO/PAMAM modified at pH = 0.

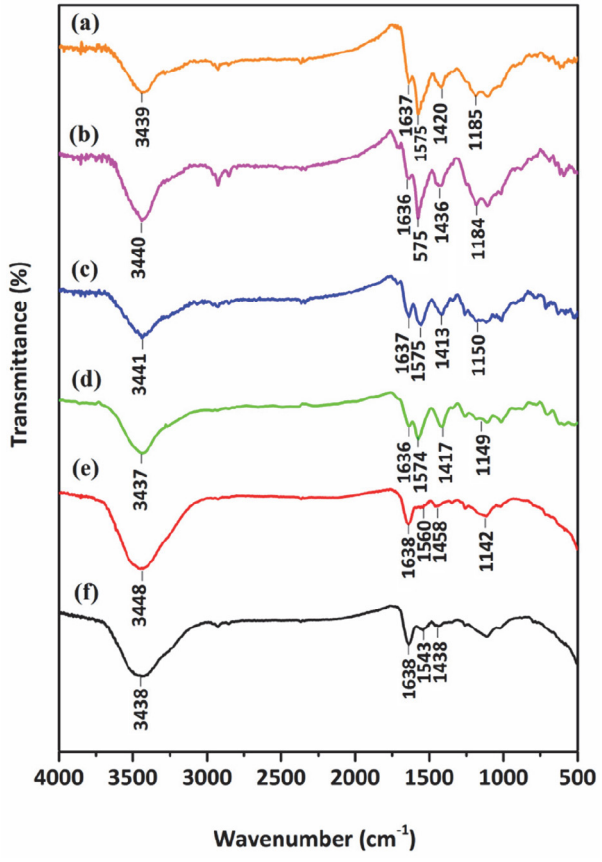

Figure 3. IR spectra of (a) pristine GO/PAMAM, (b) GO/PAMAM modified at pH = 0 and ARS–adsorbed GO/PAMAM at (c) pH = 0, (d) pH = 2, (e) pH = 5 and (f) pH = 10.

Chemical analysis of pristine GO/PAMAM by a ECS 4010 CHNS–O elemental analyzer showed that this compound contains 17.22% nitrogen, 64.02% carbon and 4.39% hydrogen by mass, Figure S4.

2. 4. Adsorption Experiments, Equations and Models

Adsorption capacity relation, adsorption experiment details, kinetic and thermodynamic equations and models used for analysis of adsorption experiments and all symbols and abbreviations were explained in detail in Supplementary Materials, Figures S5 and S6.[26,32–38]

3 Results and Discussion

3. 1. Thermodynamics of Adsorption of ARS on GO/PAMAM

The ARS molecule has two pK_a values, pK_{a1} = 5.5 and pK_{a2} = 11.5.[39,40] This compound, under experimental conditions, at pH ≤ 3 and pHs of 11 and 13 was in the forms of ARS^- (yellow), ARS^{2-} (red) and ARS^{3-} (violet) molecules respectively, Figures 6(a) and 6(b). The chemical structure used for ARS^- was confirmed before.[41] Thus, there were one or two ARS forms in solutions within the applied pH range in this work. These ARS forms are potential species in the solution, interacting with GO/PAMAM surface.

As published,[29,42] protonated primary amine (–NH^+_3), phenolic –OH and protonated tertiary amine (–NHR^+_2) groups of GO/PAMAM started to be deprotonated at pHs higher than 9.54 and 8.24 and 4, respectively. Thus, in acidic solutions these three functional groups and in alkaline media protonated and deprotonated primary amine groups of GO/PAMAM were its probable candidate groups for the adsorption of ARS molecules. Role of the –CO–NH– (amide) groups of the GO/PAMAM in the adsorption process was studied using FTIR spectra.

The peak of stretching vibration of phenolic C–OH group at 1185.5 cm^{-1} in the IR spectrum of GO/PAMAM, Figure 3(a), shifted to 1149.1 cm^{-1} in ARS-adsorbed GO/PAMAM at pH = 0, Figure 3(c), 1149.4 cm^{-1} in ARS-adsorbed GO/PAMAM at pH = 2, Figure 3(d) and 1141.6 cm^{-1} in ARS-adsorbed GO/PAMAM at pH = 5, Figure 3(e). This red-shifting validated interaction of this group with sulfonate group of ARS^- molecules. Also, the peak of amide group in GO/PAMAM at 1637 cm^{-1}, Figure 3(a), was observed at 1637, 1637 and 1638 cm^{-1} in spectra of ARS-adsorbed GO/PAMAM at pHs of 0, 2 and 5, Figures 3(c)–3(e), respectively and did not have wavelength shift. Therefore, from FTIR spectra, it was concluded that in acidic solutions –NH^+_3 and phenolic –*OH* groups of GO/PAMAM interacted with sulfonate group of ARS^- molecules. In this work, the functional groups of GO/PAMAM that interacted with ARS molecules are called its adsorption sites.

At first, the adsorption of ARS molecules in alkaline media was studied. From its pK_{a1} and pK_{a2} value, ARS deprotonated into ARS^{2-} molecules at pH = 10 and ARS^{3-} molecules at pHs of 13 and 14, respectively. Adsorption isotherms at pHs of 10, 13 and 14 consisted of two curves, Figures 7(a) and 7(b). At pH = 10, ARS^{2-} molecules and at pH = 13, ARS^{3-} molecules interacted first with –NH^+_3 (in the first curve) and subsequently with –NH_2 (in the second curve) sites of GO/PAMAM surface, respectively.

The observed decrease in q_{sssB} value in isotherm at pH = 10 compared to isotherm at pH = 13 was resulted from a decrease in the number of –NH^+_3 groups of adsorbent surface. An increase in the negative charge of ARS molecule, as solution Ph was increased from 10 to 13, resulted in an increase in the electrostatic repulsion between adsorption sites and ARS molecules which in turn resulted in a decrease in *K* values of regions I, IIA and IIB from pH

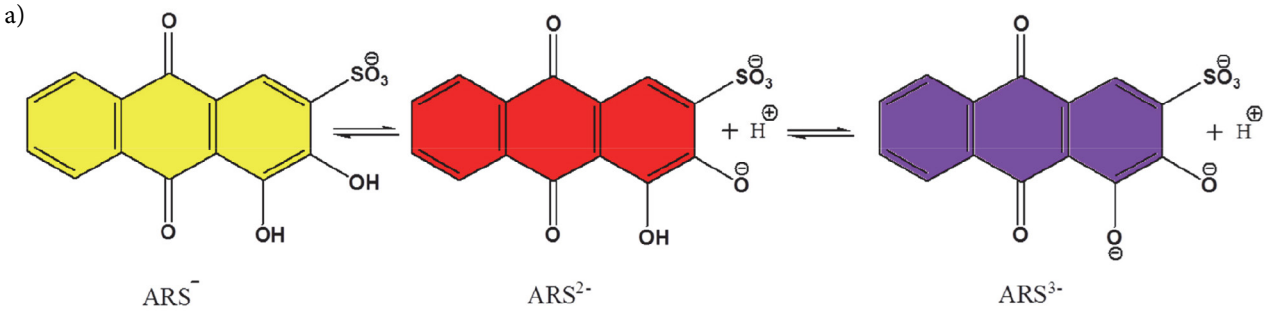

Figure 6. (a) Equilibrium relations among different types of ARS molecules at various pHs and (b) various forms of ARS molecules at (1) pH = 3, (2) pH = 5, (3) pH = 11 and pH = 13.

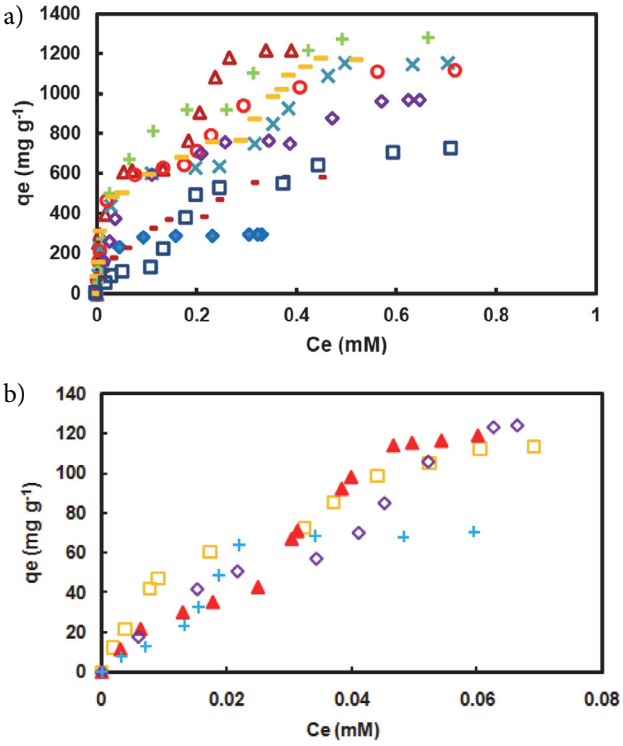

Figure 7. Adsorption isotherms of ARS on GO/PAMAM at 100 rpm and (a) at ♦ pH = 0, – pH = 0.3, Δ pH = 1, – pH = 3 and □ pH = 5 at 318 K and pH = 2 at × 308, ○ 318 and + 328 K and (b) at □ pH = 10, ▲ pH = 13 and + pH = 14 at 318 K.

= 10 to pH = 13, Table 2.

At pH = 14, ARS^{3-} molecules interacted with $-NH_2$ sites. As seen from Table 2, adsorption binding constants of ARS^{3-} molecules with $-NH_2$ site at pH = 14 (region IIA) and $-NH_2$ site at pH = 13 (region IIB) and the adsorption binding constant of ARS^{2-} molecules with $-NH_2$ site at pH = 10 (region IIB) were comparable.

In alkaline solutions, due to the low adsorption of ARS molecules on the surface, no CRAC was observed in adsorption isotherms, Table 3.

Then, the adsorption of ARS molecules on the surface of GO/PAMAM was studied in a water solution. The pH of these series of ARS solutions was about 5. Both ARS^- and ARS^{2-} species appeared in the aqueous solution, in which ARS^- was the predominate species. Under the pH environment, *Ph* and $-NH^+_3$ sites were present on the surface of adsorbent. Given that the polarity of O–H bond is stronger than that of N–H bond, in region I and IIA (the first curve), ARS^- molecules interact with *Ph* sites first and then with $-NH^+_3$ sites, respectively.

Before adding adsorbent to the solutions, the color of solutions was brown (a mixture of ARS^- and ARS^{2-} molecules). At the end of region IIB (the second curve) and $CRAC_{C2-C3}$ (the CRAC between regions IIB and IIC), the color of the solutions in region IIC (the third curve) became red that confirmed ARS^- molecules adsorbed on the surface of GO/PAMAM in regions I, IIA and IIB. With an increase in the initial concentration of solution the color became paler, Figures 8(a) and 8(b). By considering the changes in the color of ARS solutions, it was speculated that in regions I, IIA and IIB, ARS^- molecules (in brown color) adsorbed on *Ph* and then on $-NH^+_3$ sites respectively. This adsorption step is followed by ARS^{2-} molecules (in red color) adsorbed on the remaining $-NH^+_3$ sites in region IIC. As seen from experimental data in Table 2, the

Table 2. Adsorption equilibrium constants obtained from the Henry and Temkin equations based on the ARIAN model and experimental ssc_A, q_{sssA}, ssc_B, q_{sssB}, c_{max} and $q_{e,max}$ values for adsorption of ARS on GO/PAMAM in water, alkaline and acidic solutions in regions I, IIA, IIB and IIC at 100 rpm and 308–328 K.

Solvent	T	Henry (region I)			Temkin (region IIB)			Temkin (region IIC)					
	(K)	K	ssc_B	q_{sscB}	c_2	ssc_C	q_{sscC}	c_2	c_{max}	$q_{e,max}$			
		ARS^- on *Ph* site			ARS^- on $-NH^+_3$ site			ARS^- on $-NHR^+_2$ site					
pH = 0	318	3.32×10^7	2.25×10^{-3}	72.7	1.55×10^6	0.16	291.1	–	–	–	–	–	–
pH = 0.3	318	8.41×10^6	1.29×10^{-2}	107.9	1.96×10^5	0.21	380.4	1.58×10^4	0.37	575.6	–	–	–
pH = 1	318	7.19×10^7	3.56×10^{-3}	252.6	2.26×10^5	0.18	759.6	1.08×10^4	0.27	1182.6	–	–	–
pH = 2	308	4.95×10^7	4.45×10^{-3}	222.7	1.73×10^6	0.25	636.7	7.39×10^3	0.38	929.4	–	–	–
	318	3.22×10^7	4.81×10^{-3}	154.7	6.19×10^5	0.18	633.2	1.60×10^4	0.41	1027.6	–	–	–
	328	1.09×10^7	7.03×10^{-3}	133.7	2.85×10^5	0.18	919.3	2.36×10^4	0.49	1275.2	–	–	–
pH = 3	318	3.09×10^7	4.96×10^{-3}	154.2	8.43×10^5	0.23	754.2	9.26×10^3	0.39	1091.5	–	–	–

Adsorption in		Henry (region I)[A]			Temkin (region IIA)[A]			Temkin (region IIB)[B]			Temkin (region IIC)[C]		
		K	ssc_A	q_{sscA}	c_2	ssc_B	q_{sscB}	c_2	ssc_C	q_{sscC}	c_2	c_{max}	$q_{e,max}$
pH = 5*	318	2.47×10^6	3.15×10^{-2}	79.1	2.39×10^5	0.16	291.1	1.15×10^4	0.38	544.3	1.49×10^4	0.45	637.0
pH = 10*[D]	318	5.70×10^6	3.74×10^{-3}	21.4	7.29×10^5	0.03	72.6	9.98×10^4	6.5×10^{-2}	112.5	–	–	–
pH = 13*[D]	318	3.50×10^6	6.19×10^{-3}	21.7	6.66×10^5	0.02	42.8	5.86×10^4	4.7×10^{-2}	114.0	–	–	–
pH = 14*[E]	318	1.71×10^6	1.32×10^{-2}	23.3	9.94×10^4	0.03	63.7	–	–	–	–	–	–

Units of K and c_2 are in mg g^{-1} M^{-1} and M^{-1}. Units of ssc_A, ssc_B, ssc_C and c_{max} are in mg. Units of q_{sscA}, q_{sscB}, q_{sscC} and $q_{e,max}$ are in mg g^{-1}. *Adsorption sites and ARS types at these pHs are discussed in text. [A]Regions I and IIA are in the first curve (Ph site). [B]Region IIB is in the second curve ($-NH^+_3$ site). [C]Region IIC is in the third curve ($-NHR^+_2$ site). [D]At pHs of 10 and 13, $q_{sscC} = q_{e,max}$ and $ssc_c = c_{max}$. [E]At pH = 14, $q_{sscB} = q_{e,max}$ and $ssc_B = c_{max}$.

Table 3. CRACs for the adsorption of ARS on GO/PAMAM in water, alkaline and acidic solutions at 100 rpm and 308–328 K.

Solvent	*T* (K)	ssc_B (mM)	$CRAC_{C1-C2}$ (mM)	– –	ssc_C (mM)	c_{max} (mM)	$q_{e,max}$ (mg g^{-1})
pH = 0	318	2.25×10^{-3}	–	–	0.16	0.16	291.1
pH = 0.3	318	1.29×10^{-2}	0.14–0.21	–	0.21	0.37	575.6
pH = 1	318	3.56×10^{-3}	0.07–0.18	–	0.18	0.27	1182.6
pH = 2	308	4.45×10^{-3}	0.20–0.25	–	0.25	0.38	929.4
	318	4.81×10^{-3}	0.14–0.18	–	0.18	0.41	1027.6
	328	7.03×10^{-3}	0.18–0.26	–	0.18	0.49	1275.2
pH = 3	318	4.96×10^{-3}	0.23–0.29	–	0.23	0.39	1091.5
Solvent	***T***	ssc_A	ssc_B	$CRAC_{C2-C3}$	ssc_C	c_{max}	$q_{e,max}$
pH = 5	318	3.15×10^{-2}	0.11	0.25–0.38	0.38	0.45	637.0
Solvent	***T***	ssc_A	$CRAC_{C1-C2}$	ssc_B	ssc_C	c_{max}	$q_{e,max}$
pH = 10	318	3.74×10^{-3}	–	3.2×10^{-2}	–	6.5×10^{-2}	112.5
pH = 13	318	6.19×10^{-3}	–	2.5×10^{-2}	–	4.7×10^{-2}	114.0
pH = 14	318	1.32×10^{-2}	–	–	–	3.4×10^{-2}	63.7

ssc_A, ssc_B, $ssc_C$are the starting concentrations of regions IIA, IIB and IIC respectively and their units are in mM. $CRAC_{C1-C2}$ and $CRAC_{C2-C3}$ are the concentration range of leveling off the adsorption isotherm between the first and second and the second and third curves, respectively and their unit is in mM.

maximum adsorption capacity of regions I and IIA is q_{sscB} = 291,1 mg g^{-1}, which was much bigger than those of reported for ARS[43] and orange IV[44] which interacted with

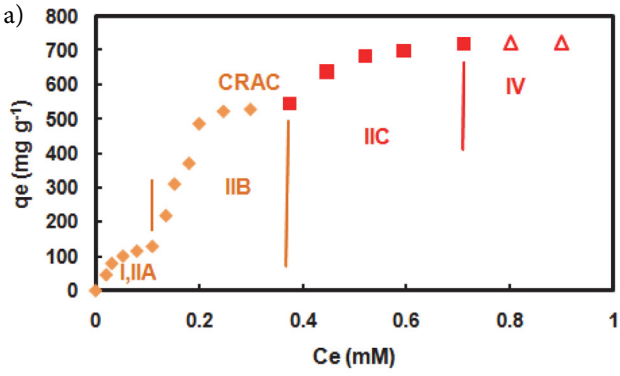

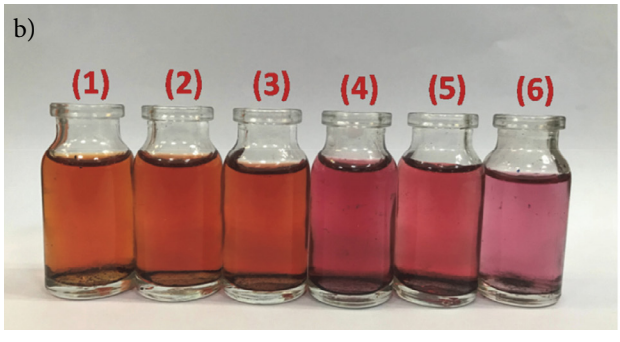

Figure 8. (a) Adsorption isotherm of ARS on GO/PAMAM at pH = 5 which showed adsorption of ARS^- molecules on *Ph* (region I) and $-NH^+_3$ (region IIA) sites and ARS^{2-} molecules on $-NH^+_3$ (region IIB) sites, respectively. (b) Solutions in bottles 1-3 belonged to regions I, IIA and the second CRAC. Solutions in bottles 4-6 belonged to region IIB and initial ARS concentrations increased from bottles 1 to 6.

GO. However, our q_{sscB} was smaller than that of the second and third curves, $q_{max,e} - q_{sscB}$ = 345,9 mg g^{-1}, Table 2. Then, it was concluded that in region IIC, ARS^{2-} molecules interacted with some remaining $-NH^+_3$ sites.

As seen from Table 2, at pH = 5 and 318 K, ARS^- in region IIB and then ARS^{2-} in region IIC interacted with $-NH^+_3$ sites. The *K* value of the former interaction was higher than the latter one. Given the negative charge of $ARS^{2-}$was higher than that of ARS^-, the *K* values observed in region IIC were less than those in region II, Figures 8 and 9. The observation of K values was attributed from two aspects: (1) the steric hindrance caused by the adsorbed ARS molecules; (2) increasing repulsion interaction between ARS molecules and negatively charged adsorbent surface.

Alizarin (AZ) was used to determine the functional group responsible for interacting ARS with GO/PAMAM in alkaline media. AZ molecule shares the same structure as ARS except for the missing sulfonate group, Figure 10. The pK_a of AZ is 6.77 and both hydroxyl groups of AZ are ionized under an alkaline environment.[45] Experiments showed that AZ adsorption capacity of GO/PAMAM at pH = 12 was 21.6 mg g^{-1} that was much less than the ARS adsorption capacity of 113.4 mg g^{-1} under similar conditions. This test verified that the sulfonate group of ARS^{2-} and ARS^{3-} molecules but not their $-O^-$ groups interacted with GO/PAMAM in alkaline media.

Finally, the adsorption of ARS on GO/PAMAM was studied in acidic solutions, pH ≤ 3. Visible spectroscopy technique showed that only ARS^- molecules appeared in this range of pHs. As reported before,[42] with the decrease in pH (pH < 4) all the tertiary amines were protonated. Due to the repulsion between primary and tertiary amines of PAMAM dendrimer, its structure was opened, yielding

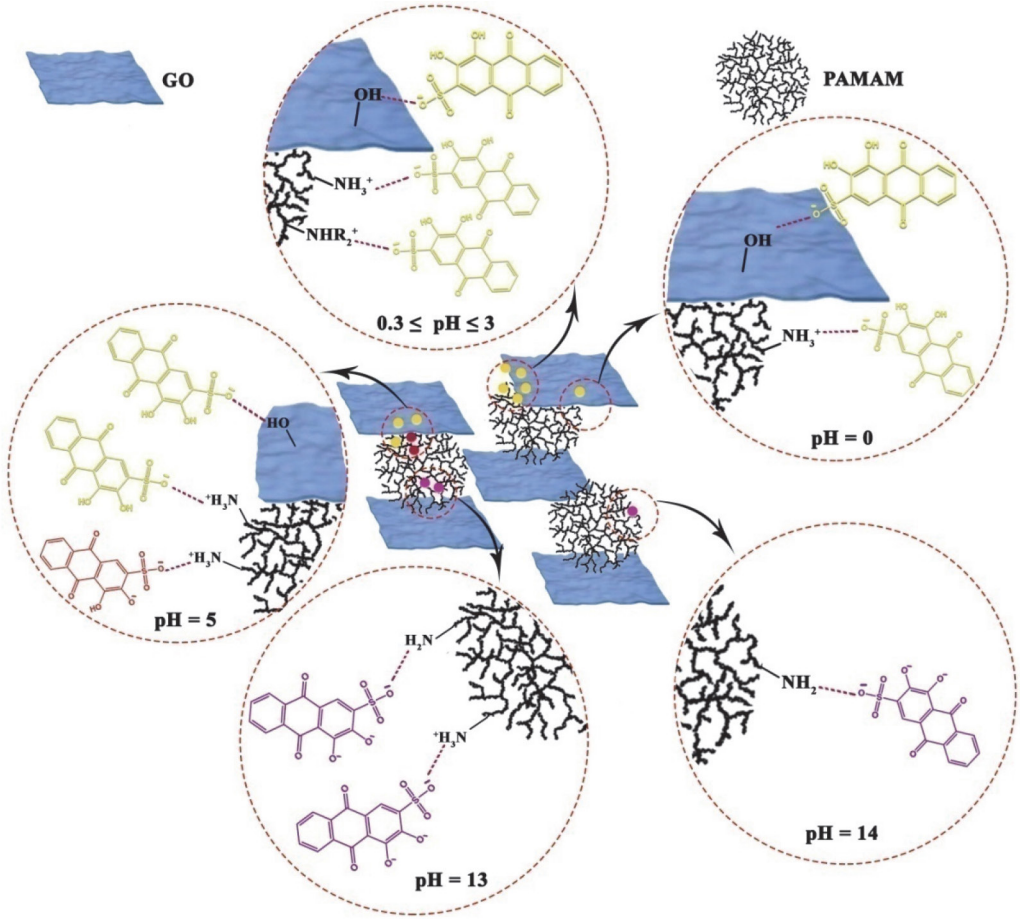

Figure 9. Adsorption sites of GO/PAMAM for different types of ARS molecules at different pHs.

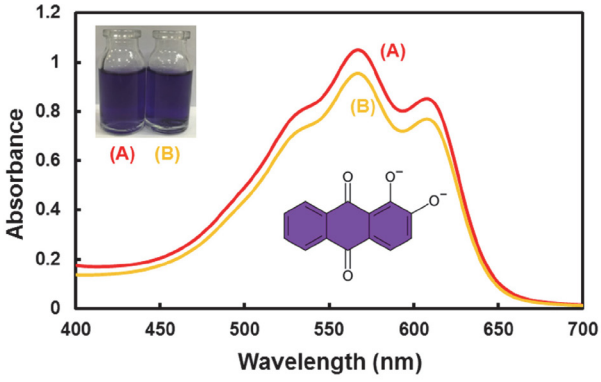

Figure 10. Absorption spectra of (A) 0.1 mM AZ and (B) 0.1 mM AZ in the presence of 0.001 g GO/PAMAM. The molecular structure of AZ at pH = 12 is shown in this figure.

an ideal interaction between the *Ph* groups of GO moiety of adsorbent and ARS^- molecules. Thus, the adsorption of ARS on the pristine GO/PAMAM obeyed only from the Henry equation (region I) without forming region IIA. Under these conditions more primary and tertiary amine groups exposed to ARS^- molecules. Due to binding three alkyl groups to N atom of tertiary amines, the polarity of N–H bond of protonated tertiary amines form is less than that for N–H bond of protonated primary amines $-NH^+_3$ and O–H bond of *Ph* groups.

As shown in Tables 2, S1–S3 and Figure 7, the adsorption of ARS^- molecules at pH≤ 3 occurred in three regions (I, IIB and IIC). However, the adsorption of ARS^- molecules at pH = 0 happened in two regions (I and IIB) and their related adsorption isotherms were formed from two curves.

Thus, ARS^- molecules adsorbed on *Ph*, $-NH^+_3$ and $-NHR^+_2$ sites in region I and sections IIB and IIC, respectively. As shown in Tables 2, 3, S1–S3 and Figures 7(a) and 7(b), the maximum experimental adsorption capacity ($q_{e,max}$) of the adsorption of ARS^- molecules on GO/PAMAM at pHs of 1, 2 and 3 were comparable. This implied that an increase in ionic strength of solutions at pHs from 3 to 1 did not affect the $q_{e,max}$ of process. The adsorption binding constants (K) in regions I and IIB at 318 K increased from pHs 1 to 3. However, K values in region IIC (on the $-NH^+_3$ sites) were approximately constant. Each of the adsorption isotherms at pHs of 1, 2 and 3 consisted of two curves and a CRAC appeared between them, Table 3. The presence of

CRACs was due to the high adsorption capacity of adsorbent for ARS^- molecules in the concentration range of the first curve which resulted in steric hindrance of adsorbed ARS^- molecules on the adsorbent surface and electrostatic repulsion between adsorbent surface and ARS^- molecules.

At pH = 2, thermodynamic parameters of interaction of ARS^- molecules with *Ph*, $-NH^+_3$ and $-NHR^+_2$ sites in regions I, IIB and IIC respectively, were calculated using the adsorption binding constants obtained from the Henry, Temkin and Temkin isotherms respectively, Table 2. ΔH and ΔS values were 63.2 kJ mol^{-1} and –57.1 J mol^{-1} K^{-1} in region I, 75.8 kJ mol^{-1} and –127.2 J mol^{-1} K^{-1} in region IIB and 48.9 kJ mol^{-1} and 237.8 J mol^{-1} K^{-1} in region IIC, respectively.

Afterwards, the Thermodynamic parameters of the adsorption were analyzed. Adsorption in the liquid phase, occurred through two kinds of interactions. One of them is the interaction of adsorbate molecules with surface of adsorbent and the other is due to replacing water molecules attached to the surface by adsorbate molecules.

The former interaction, by immobilization of adsorbate molecules, lowers the entropy of adsorption system. The latter one increases the disorder and thus the entropy of adsorption system which is result of the mobility of detached water molecules. At pH = 2, the negative ΔS values observed in adsorption of ARS^- molecules on the surface of GO/PAMAM in region I and sections IIB, showed electrostatic (ion-ion or ion-dipole) interaction occurred between ARS^- molecules with *Ph* and $-NH^+_3$ adsorption sites of GO/PAMAM. The negative ΔH values of these interactions indicated that the adsorption process in these two regions were exothermic.

On the other hand, the large positive ΔS value in region IIC showed after initial electrostatic interaction between ARS^- molecules and $-NHR^+_2$ adsorption sites of GO/PAMAM surface, a hydrophobic interaction happened between ARS^- molecules and hydrocarbon chains of $-NHR^+_2$ adsorption site that detached a large number of water molecules solvating ARS^- molecules and GO/PAMAM surface. The positive sign of ΔH value of this interaction was due to: (1) required energy to separate more number of water molecules from the GO/PAMAM surface and ARS^- molecules and (2) subsequent hydrophobic interactions between ARS^- molecules and GO/PAMAM surface.[46,47]

It was observed that adsorption capacities of these two curves of isotherms (specially the second curve) decreased from pH = 1 to pH = 0. Adsorption capacities of the second curve decreased about 50% from pH = 1 to pH = 0.3 and further disappeared at pH = 0 which showed gradual decrease in the availability of the second adsorption site with an increase of HCl concentration.

This observation was further investigated using the following tests. The comparison of EDS spectra of ARS–adsorbed GO/PAMAM modified by 1 M HCl for 10 hours and pristine GO/PAMAM showed that atomic percentages of nitrogen were comparable, which were 24.75% and 23.13% in the former and latter samples, respectively (without considering atomic percentage of its chlorine), Figures S3(a) and S3(b).

According to the measurements of nitrogen physisorption BET technique for pristine GO/PAMAM, ARS-adsorbed GO/PAMAM at pH = 2 and ARS-adsorbed GO/PAMAM at pH = 0, BET surface area, maximum pore volume for slit pore geometry, adsorption average pore diameter (by BET) and pore volume were 9.59 m^2 g^{-1}, 0.0044 cm^3 g^{-1}, 18.9 nm and 0.045 cm^3 g^{-1} for the first sample, 1.92 m^2 g^{-1}, 0.001 cm^3 g^{-1}, 14.2 nm and 0.0069 cm^3 g^{-1} for the second sample and 1.35 m^2 g^{-1}, 0.0006 cm^3 g^{-1}, 10.7 nm and 0.0036 cm^3 g^{-1} for the third sample respectively, Figures S1(a)-S1(c). The t-plot micropore area for ARS-adsorbed GO/PAMAM at pH = 0 was 0.0075 m^2 g^{-1} and ARS-adsorbed GO/PAMAM at pH = 2 and pristine adsorbent were lack of micropores. These results showed that as GO/PAMAM at pH = 0 adsorbed less ARS molecules than GO/PAMAM at pH = 2, the BET surface area and slit pore volume of adsorbent at pH = 0 were less than those values at pH = 2 and part of adsorbent pores at pH = 0 changed to micropores.

The comparison of IR spectra of ARS-adsorbed GO/PAMAM modified by 1 M HCl for 10 hours and pristine GO/PAMAM showed that those IR spectra were very similar, Figures 3(a) and 3(b). Also, the shift of broad peak around 2θ of 26.7° in the XRD spectrum of GO/PAMAM to 26.4° in the XRD spectrum of GO/PAMAM modified at pH = 0 showed a change in the structure of the latter one, Figures 2(a) and 2(b).

This evidence confirmed that the decrease in the adsorption capacities of the first and second curves of adsorption isotherms at pHs of 0.3 and 0 was due to masking the adsorption sites of GO/PAMAM. Indeed, a decrease in pH to less than 1 and an increase in ionic strength of solutions resulted in a shrinkage in PAMAM structure[42] and possible interactions were between $-NH^+_3$ and polyamide groups of PAMAM dendrimer and between functional groups of PAMAM with a number of functional groups on the GO planes of adsorbent like its C = C bonds and compressed its structure. This resulted in a decrease in the number of free *Ph* and $-NH^+_3$ groups and entrapment of $-NHR^+_2$ groups in internal structure of PAMAM and thus, resulted in a decrease in the availability of *Ph*, $-NH^+_3$ and $-NHR^+_2$ adsorption sites of GO/PAMAM for ARS^- molecules.

Finally, relative adsorption capacities of isotherms for regions I $\left(\frac{q_{sscA}}{q_{e,\max}}\right)$, IIA $\left(\frac{q_{sscB}-q_{sscA}}{q_{e,\max}}\right)$, IIB $\left(\frac{q_{sscC}-q_{sscB}}{q_{e,\max}}\right)$ and IIC $\left(\frac{q_{e,\max}-q_{sscC}}{q_{e,\max}}\right)$ were given in Table S4. For example, because at pH = 5 the concentration of ARS^{2-} molecules was less than ARS^- molecules, the adsorbent's relative adsorption capacity for ARS^{2-} (region IIC) was 0.15 of $q_{e,\max}$ value.

3. 2. Kinetics of Adsorption of ARS on GO/PAMAM

The adsorption mechanism of ARS on GO/PAMAM was studied by the KASRA model, and intraparticle diffusion and ISO equations using different ARS initial concentrations, temperatures, pHs and shaking rates. At 318 K, using 0.25 mM ARS at pH = 0 and using 0.07 mM ARS at pH = 2, only one adsorption curve was observed in their kinetic diagrams without the presence of TRAK, implying that the adsorption of ARS^- molecules occurred on the *Ph* sites of adsorbent, Figures 11(a) and 11(b) and Table 4.

gions (curves) were observed in all kinetic diagrams: ARS^- molecules interacted with *Ph* sites in the first curve, followed by interaction with $-NH^+_3$ and $-NHR^+_2$ sites in the second one. It was observed that at pH = 2, ISO rate constants for the adsorption on the *Ph* sites (in the first region) increased with an increase of the shaking rate. Also, an increase in pH from 2 to 3 increased the ISO rate constants for the adsorption on *Ph*, $-NH^+_3$ and $-NHR^+_2$ sites.

At pH = 2, adsorption acceleration, initial velocity and k_{dif} for adsorption on *Ph*, $-NH^+_3$ and $-NHR^+_2$ sites increased with temperature, shaking rate and ARS initial concentration. The k_{I1} values at 0.7 mM and 100 rpm, that

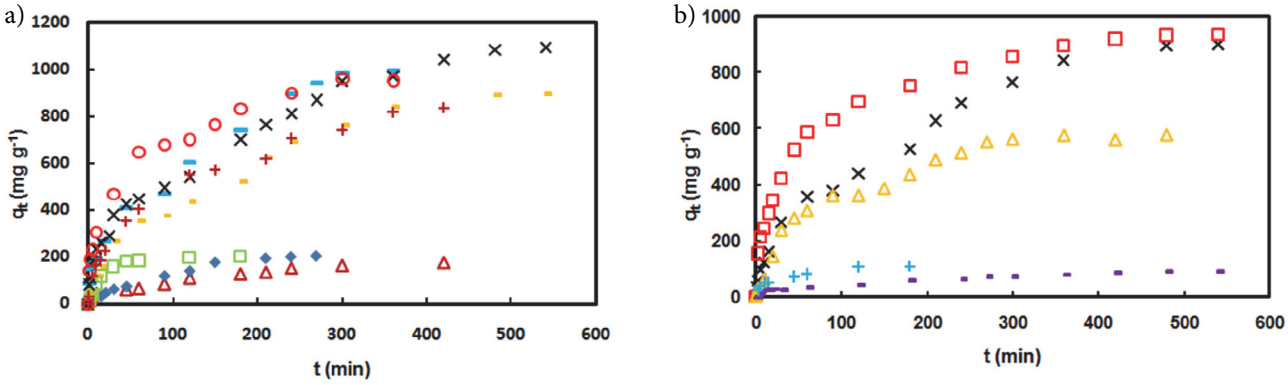

Figure 11. Kinetic curves of adsorption of ARS on GO/PAMAM (a) at ♦ pH = 0 and 0.25 mM ARS and □ pH = 2 and 0.07 mM ARS at 318 K and 100 rpm; at pH = 2, 0.7 mM ARS and – 308, × 318 and ○ 328 K at 100 rpm; at Δ pH = 2, 0.07 mM ARS, 318 K and 100 rpm; at pH = 2, 0.7 mM ARS and 318 K at - 40 and + 70 rpm, respectively and (b) at × pH = 2, 0.7 mM ARS, 318 K and 40 rpm; at □ pH = 3 and 0.7 mM ARS, Δ pH = 5 and 1 mM ARS, - pH = 10 and 0.07 mM ARS and + pH = 13 and 0.07 mM ARS at 318 K and 100 rpm.

Table 4. TRAKs for adsorption of ARS on GO/PAMAM in water, alkaline and acidic solutions at 100 rpm and 308–328 K.

Solvent	T (K)	$[ARS]_0$ (mM)	rpm	$TRAK_{C1-C2}$ (min)	$q_{TRAKC1-C2}$ (mg g^{-1})	t_e (min)	q_e (mg g^{-1})
pH = 0	318	0.25	100	–	–	270	206.3
pH = 2	318	0.07	100	–	–	180	202.3
(0.1 M NaCl)	318	0.07	100	–	–	420	174.0
	308	0.70	100	–	–	360	991.9
	318	0.70	100	–	–	420	965.9
	328	0.70	100	–	–	300	960.1
	318	0.70	70	–	–	360	815.4
	318	0.70	40	–	–	480	893.4
pH = 3	318	0.70	100	–	–	480	931.5
pH = 5	318	1.00	100	90–120	362.2–362.5	360	577.8
pH = 10	318	0.07	100	10–30	25.7–27.1	480	90.4
pH = 13	318	0.07	100	10–15	51.6–53.7	120	109.0

$TRAK_{C1-C2}$ is the TRAK between the first and second kinetic curves. t_e is the time of starting plateau.

As seen from Tables 5 and 6 and S5–S7, adsorption acceleration, initial velocity, k_{dif}, k_{I1} and k_{I2a} decreased as pH decreased from 2 to 0. This was resulted from the compression of the adsorbent structure at pH = 0, that blocked interior adsorption sites. Using 0.7 mm ARS at pHs of 2 and 3 at different shaking rates and temperatures two re-

implied the interaction of *Ph* sites with ARS^- molecules increased with temperature. The activation energy of the adsorption in region I was 114.5 kJ mol^{-1}. Therefore the adsorption of ARS on *Ph* sites was reaction-controlled. The adsorption in region I in region I only spanned about 6–8% of the whole adsorption duration but was accounted

Table 5. Coefficients of the intraparticle diffusion equation for kinetics of ARS adsorption on GO/PAMAM at different temperatures and in various shaking rates and ARS initial concentrations.

Solvent	T (K)	$[ARS]_0$ (mM)	rpm	KASRA region 1 (1st curve) k_{dif}	a_1	(t_2, q_2)	KASRA region 2 (1st curve) k_{dif}	a_2	TRAK	KASRA region 2 (2nd curve) (t_3, q_3)	k_{dif}	a_3	TRAK
Corresponding to thermodynamic				**ARIAN region I**			**ARIAN section IIB**			**ARIAN section IIC**			
At $pH \leq 3$ adsorption of ARS^- on				***Ph* site**			**$-NH^+_3$ site**			**$-NHR^+_2$ site**			
pH = 0	318	0.25	100	11.2	−0.048	(45,73.7)	14.1	-4.0×10^{-3}	–	–	–	–	–
pH = 2	318	0.07	100	**32.6**	**−0.23**	**(45,181.8)**	**3.2**	$\mathbf{-2.0 \times 10^{-3}}$	**Adsorption only on *Ph* site**		–		–
(0.1 M NaCl)	318	0.07	100	**19.2**	**−0.47**	**(10,44.8)**	**8.2**	$\mathbf{-1.6 \times 10^{-3}}$	**Adsorption only on *Ph* site**		–		–
	308	0.70	100	97.1	−10.40	(5,169.9)	44.3	−0.11	–	(90,469.2)	56.2	−0.012	–
	318	0.70	100	82.5	−14.28	(5,184.2)	50.7	−0.13	–	(60,449.2)	45.4	−0.006	–
	328	0.70	100	105.7	−16.94	(5,232.6)	65.0	−0.14	–	(90,681.0)	37.9	−0.004	–
	318	0.70	70	66.3	−4.00	(9,120.6)	52.5	−0.08	–	(60,402.8)	35.3	−0.002	–
	318	0.70	40	43.8	−2.40	(10,120.1)	38.4	−0.11	–	(90,376.7)	44.9	−0.004	–
pH = 3	318	0.70	100	119.4	−8.45	(5,213.8)	71.6	−0.11	–	(60,585.1)	24.9	−0.002	–
pH = 5*	318	1.00	100	24.9	−1.19	(10,61.8)	75.0	−0.106	–	(30,237.0)	70.1	−0.006	90–120

Solvent	T (K)	$[ARS]_0$ (mM)	rpm	KASRA region 1 (1st curve) k_{dif}	a_1	(t_2, q_2)	a_2	TRAK	KASRA region 2 (2nd curve) (t_3, q_3)	k_{dif}	a_3	TRAK
Corresponding to thermodynamic				**ARIAN region I and section IIA**					**ARIAN section IIB**			
pH = 10*	318	0.07	100	7.7	−0.65	–	–	–	10–30	(30,27.1)	4.0	-4.0×10^{-4} –
pH = 13*	318	0.07	100	19.8	−0.95	–	–	–	10–15	(15,53.7)	7.8	-4.0×10^{-3} –

Unit of k_{dif} is in mg g^{-1} $min^{-0.5}$. Units of a_1, a_2 and a_2 are in mg g^{-1} min^{-2}. Units of t_1, t_2 and t_3 are in min and those of q_1, q_2 and q_3 are in mg g^{-1} and $t_1 = q_1 = 0$. Boundary points coordinates of diffusion regions, (t_n, q_n), are similar to those of the KASRA model, (t_{0n}, q_{0n}) in Table S5. *At pH = 5, data from left to right belong to the first and second kinetic curves and the third kinetic curve (corresponding to the ARIAN section IIC) starts after second TRAK (90–120 min) and for that k_{dif} and $a_4$are 36.3 mg g^{-1} $min^{-0.5}$ and −0.006 mg g^{-1} min^{-2}, respectively. Adsorption sites and ARS types involved at pHs = 5, 10 and 13 are discussed in text.

Table 6. Coefficients of region 1 and region 2 (parts 2*a* and 2*b*) of the ISO equation for kinetics of ARS adsorption on different sites of GO/PAMAM at 308–328 K.

Solvent	T (K)	$[ARS]_0$ (mM)	rpm	k_{I1}	KASRA regions 1 and 2 (1st curve) k_{I2a}	k_{I2b}	$([ARS]_E, t_E, q_E)$	k_{I2a}	k_{I2b}	KASRA region 2 (2nd curve) $([ARS]_e, t_e, q_e)$
Corresponding to thermodynamic							**ARIAN region I and section IIA**			
At $pH \leq 3$ adsorption of ARS^- on				***Ph* site**		**$-NH^+_3$ site**			**$-NHR^+_2$ site**	
pH = 0	318	0.25	100	2.83×10^4	8.43×10^3	2.32×10^4	–	–	–	(0.196,270,206.3)
pH = 2	318	0.07	100	$\mathbf{3.91 \times 10^5}$	$\mathbf{1.87 \times 10^5}$	–	**Adsorption only on *Ph* site**		–	$(2.27 \times 10^{-2}$, 180,202.2)
(0.1 M NaCl)	318	0.70	100	$\mathbf{6.46 \times 10^4}$	$\mathbf{1.44 \times 10^4}$	$\mathbf{9.33 \times 10^4}$	**Adsorption only on *Ph* site**		–	$(2.42 \times 10^{-2}$, 420,174)
	308	0.70	100	1.69×10^4	1.83×10^4	3.89×10^4	(0.59,90,469.2)	1.40×10^4	5.39×10^4	(0.49,360,991.9)
	318	0.70	100	8.57×10^4	1.70×10^4	7.11×10^4	(0.556,60,449.2)	1.39×10^4	7.86×10^4	(0.418,420,965.9)
	328	0.70	100	2.57×10^5	2.88×10^4	7.84×10^4	(0.521,90,681.0)	9.81×10^3	2.21×10^4	(0.391,300,960.1)
	318	0.70	70	6.55×10^4	1.66×10^4	2.99×10^4	(0.606,60,402.8)	6.12×10^3	1.22×10^4	(0.533,360,815.4)
	318	0.70	40	3.15×10^4	3.19×10^4	–	(0.59,90,376.7)	8.76×10^3	6.57×10^4	(0.204,480,893.4)
pH = 3	318	0.70	100	1.27×10^5	6.23×10^3	1.35×10^4	(0.563,60,585.1)	7.73×10^3	1.15×10^4	(0.482,480,931.5)
pH = 5*	318	1.00	100	1.78×10^4	1.75×10^4	1.11×10^4	(0.85,90,362.2)	7.81×10^3	1.77×10^4	(0.814,360,577.8)
pH = 10**	318	0.07	100	1.98×10^5	–	–	$(6.32 \times 10^{-2}$, 10,25.7)	3.70×10^3	9.25×10^3	$(4.89 \times 10^{-2}$, 480,90.4)
pH = 13***	318	0.07	100	2.35×10^5	–	–	$(5.79 \times 10^{-2}$, 10,51.6)	3.59×10^4	1.14×10^5	$(5.21 \times 10^{-2}$, 180,110.0)

$[ARS]_E$, t_E and q_E are ARS concentration, time and adsorption capacity at the end of adsorption on a type of adsorption site, respectively (corresponding to $[ARS]_e$, t_e and q_e in the last curve). $[ARS]_e$, t_e and q_e are ARS concentration, time and adsorption capacity at the beginning of the plateau. Units of k_{I1}, k_{I2a} and k_{I2b} are in min^{-1}. $[ARS]_E$ and $[ARS]_e$ are in mM. *At pH = 5, data from left to right belong to the adsorption of ARS^- on *Ph* sites (1st kinetic curve), ARS^- on–NH^+_3 sites (2nd kinetic curve) and ARS^{2-} on –NH^+_3 sites (3rd kinetic curve), respectively. **At pH = 10, data from left to right belong to the adsorption of ARS^{2-} on –NH^+_3 (1st kinetic curve) and –NH_2 sites (2nd kinetic curve), respectively. ***At pH = 13, data from left to right belong to the adsorption of ARS^{3-} on –NH^+_3 (1st kinetic curve) and –NH_2 sites (2nd kinetic curve), respectively.

for about 34–41% of the adsorption capacity of GO/PAMAM. The adsorption on Ph sites was much faster than those on the $-NH^+_3$ and $-NHR^+_2$ sites. On the other hand, under similar conditions, other rate constants obtained from the ISO equation changed randomly with temperature and thus the adsorption on the $-NH^+_3$ and $-NHR^+_2$ sites was diffusion-controlled.

At pH = 2 and 0.07 mM ARS in 0.1 M NaCl, adsorption acceleration, initial velocity and k_{I1} increased slightly compared to those values in a solution without NaCl. This was due to more availability of ARS^- molecules to internal structure of PAMAM dendrimer with the ionic strength of solution. The slight increase in k_{I1} value with an increase in the ionic strength of solution confirmed that the adsorption interaction in region I occurs between ARS^- molecules and uncharged *Ph* groups of adsorbent.

At pH = 5, 318 K and 1 mM ARS, adsorption acceleration, initial velocity, k_{dif} and k_{I1} of the adsorption on *Ph* and $-NH^+_3$ sites (first curve) were less than those at pH = 2, 318 K and 0.7 mM ARS. Because, at pH < 4, all the primary and tertiary amines were protonated and the repulsion interaction between these amine groups of PAMAM dendrimer, its structure swelled[42] to expose more adsorbent inner surface compared to that at pH = 5, Tables 5 and 6.

At 318 K and 0.07 mM ARS, ARS^{2-} molecules at pH = 10 and ARS^{3-} molecules at pH = 13 were adsorbed on $-NH^+_3$ sites (first curve) and $-NH_2$ sites (second curve) respectively. As the pH increased from 5 to 13, the electron charge density on the adsorbent surface became higher, that increased the electrostatic repulsion between ARS molecules and adsorbent surface. The repulsive interaction yielded the appearance of TRAK in the kinetic diagrams Table 4.

3. 3 Recycling ARS-adsorbed GO/PAMAM

For recycling ARS-adsorbed GO/PAMAM, several solvents were tested, such as, diethyl ether, methanol, ethanol, benzene, DMF, THF, DMSO, diethylenetriamine and alkaline and acidic aqueous solutions, none of them could extract ARS from the used adsorbent. However, we found

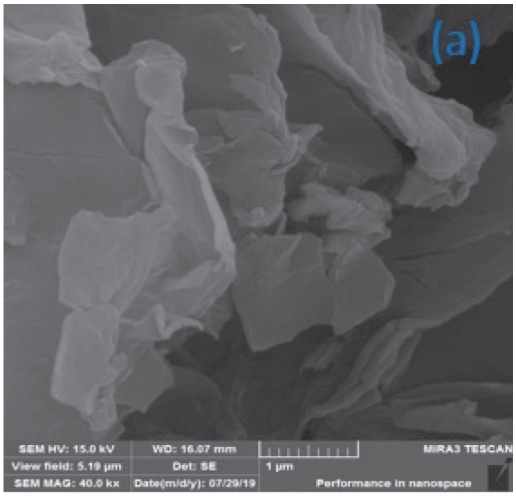

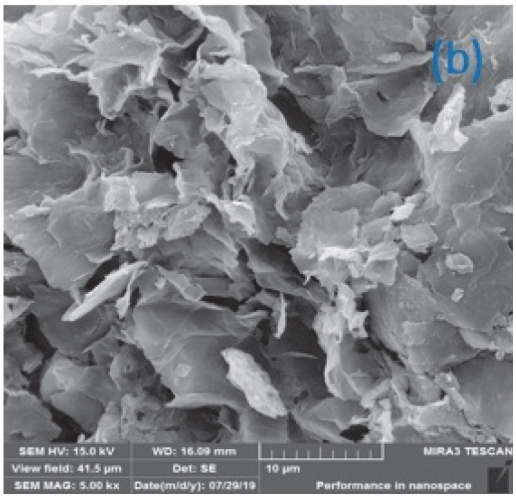

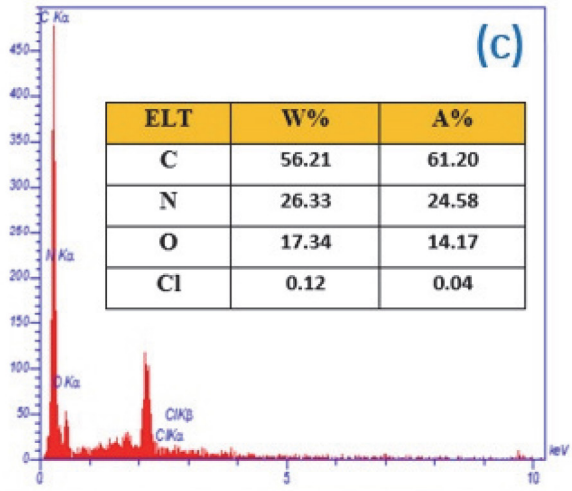

ELT	W%	A%
C	56.21	61.20
N	26.33	24.58
O	17.34	14.17
Cl	0.12	0.04

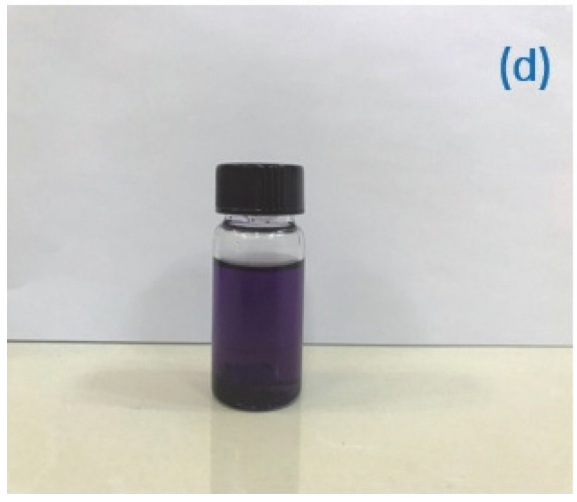

Figure 12. (a,b) SEM and (c) EDS images of the recycled GO/PAMAM and (d) extraction of ARS from the ARS-adsorbed GO/PAMAM by ethylenediamine.

ethylenediamine extracted ARS from the ARS-adsorbed GO/PAMAM very fast and effectively. In a series of experiments, 0.006 g samples of pristine GO/PAMAM were added to 30 ml of 10^{-3} M ARS solution at pH = 3 at ambient temperature. The ARS-adsorbed adsorbents were separated from supernatant after 10 h followed by washing and drying. Then, about 45 ml of ethylenediamine was added to the about 0.0025 g of the used adsorbent in three steps (15 ml/step). The adsorption capacity of pristine GO/PAMAM was fully regenerated. The EDS spectrum of the recycled adsorbent showed no trace of sulfur atom. The SEM images of the recycled adsorbent showed that its morphology was similar to that of the pristine GO/PAMAM, Figures 12(a)–12(d). Finally, ARS was separated from the ethylenediamine solution (in purple) by the distillation process.

3. 4. Selective separation of some cationic dyes from ARS using GO/PAMAM

The selective adsorption of ARS from these dyes can be used for making photochemical and electrochemical sensors.[48–50] For studying selective separation capability of dyes from ARS by GO/PAMAM, methylene blue (MB), acridine orange (AO), pyronin Y (PY), thionine (Th) and janus green B (JG) cationic and methyl blue (MEB) anionic dyes were mixed with ARS at pH = 2, Figures 13 and S5. Maximum wavelengths of ARS, MB, AO, PY, Th, JG and MEB were at 422, 664, 491, 546, 599, 820 and 599 nm, respectively.

At this pH, GO/PAMAM had its maximum adsorption capacity for ARS. Using the adopted initial ARS concentration, ARS was fully removed from the solution. Comparison of the UV-Vis spectra of pure dyes solutions with those of ARS-dye mixtures (in the absence of adsorbent) showed that the strength of dye-ARS interaction followed the trend: JG (by formation of deposit) > MB, AO, PY >Th > MEB, peaks B and D of Figures 14(b) –14(g). The final concentrations of Th, MB, AO and PY in their mixtures with ARS were 95%, 56%, 45% and 56% of their initial concentrations, respectively. As shown in peaks B and D of Figure 14(f), MEB and ARS anionic dyes do not interact together.

As shown in absorption peaks of B and C of Figures 14(b)–14(g), the final concentrations of Th, MB, AO, PY, JG and MEB after adsorption on the surface of GO/PAMAM were 67%, 84%, 83%, 93%, 70% and 22% of their initial concentrations, respectively.

But, as seen in peaks of B, E of Figures 14(b)–14(g), due to interaction of Th, MB, AO, PY and JG with adsorbed ARS on the surface of GO/PAMAM and adsorption of MEB on the surface of GO/PAMAM in the mixture of these dyes with ARS in the presence of GO/PAMAM, their final

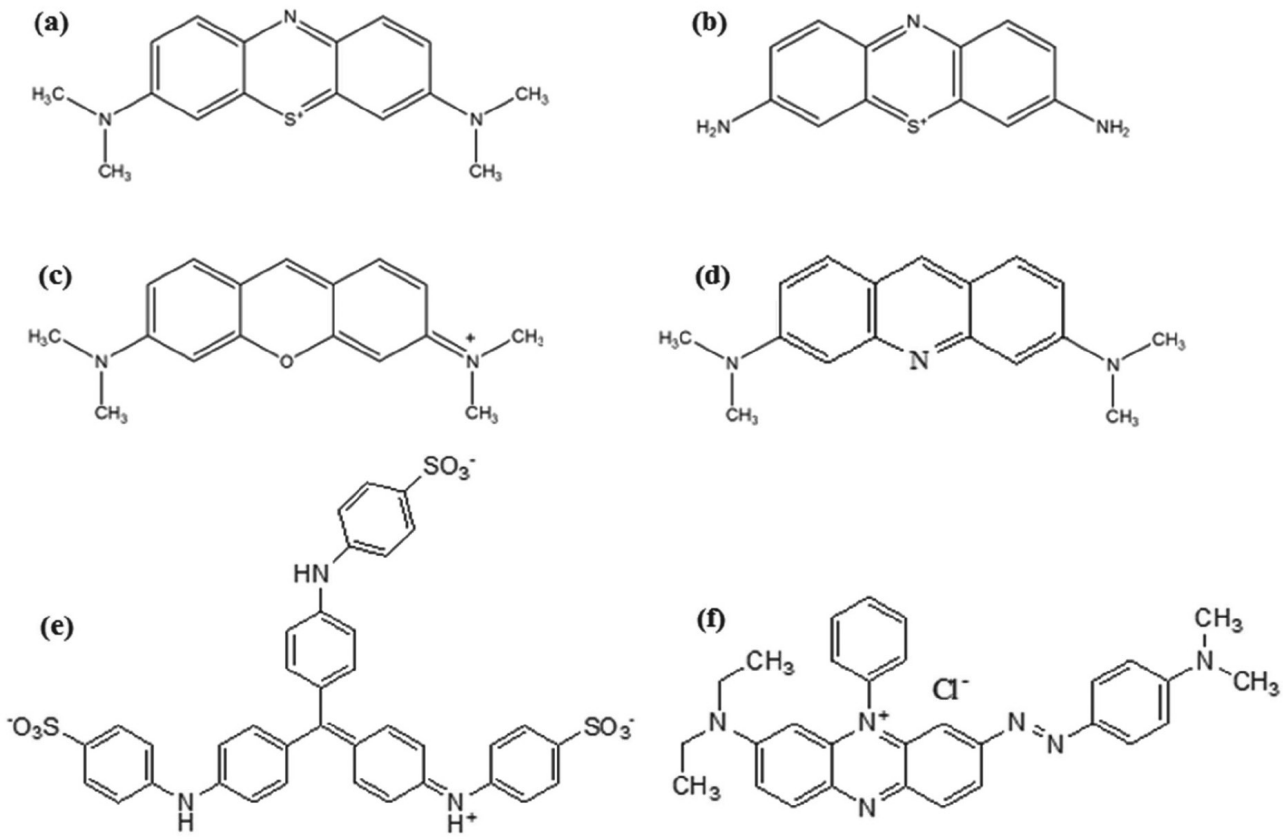

Figure 13. Molecular structure of (a) MB, (b) Th, (c) PY, (d) AO, (e) MEB and (f) JG.

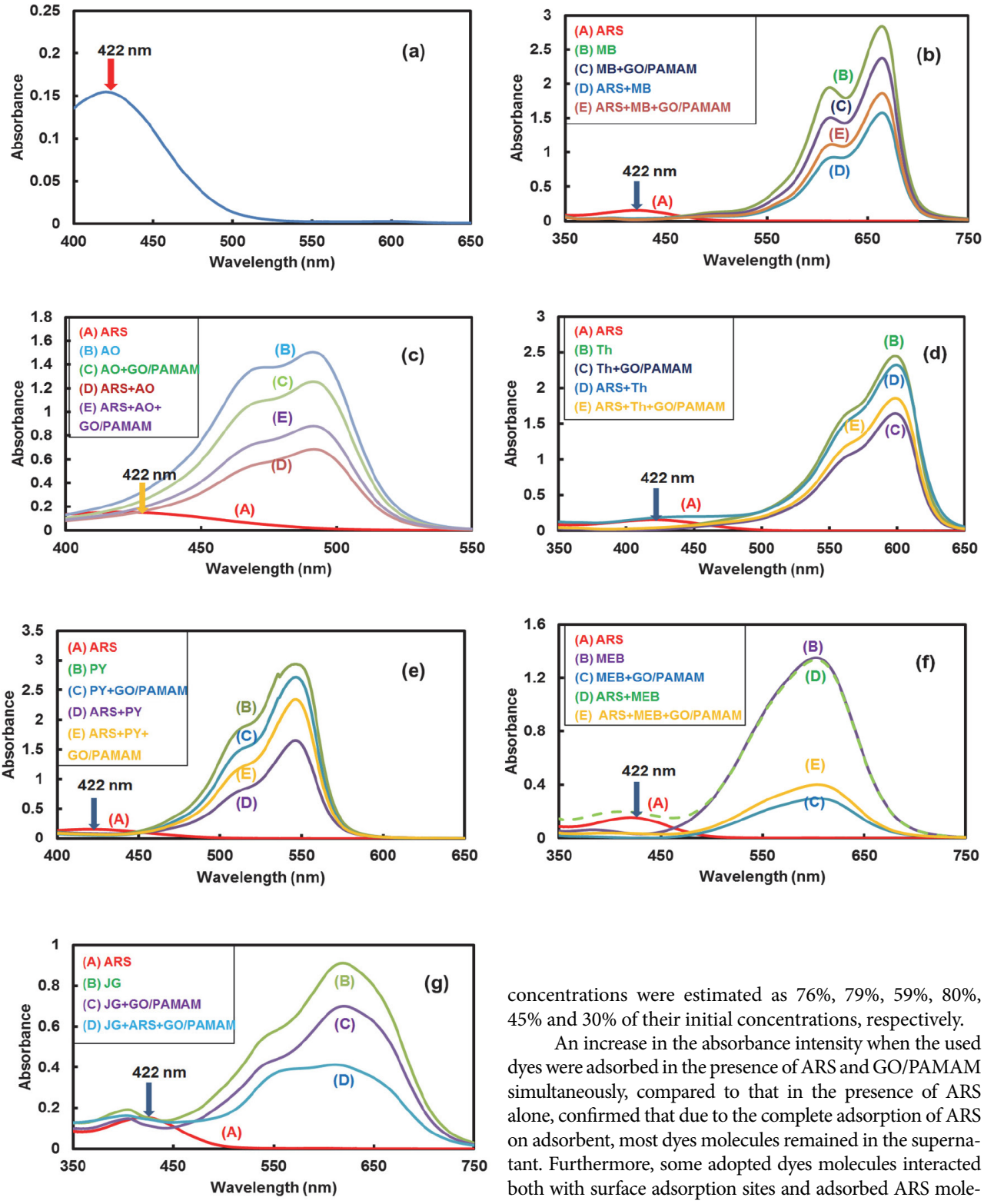

Figure 14. (a) Absorption peak of ARS at pH = 2. In all solutions, concentration of ARS was 5×10^{-2} mM and those of MB in (b), AO in (c), Th in (d), PY in (e) and MEB in (f) were 5×10^{-2} mM and concentration of JG in (g) was 2.5×10^{-2} mM. Tests were carried out at pH = 2 and room temperature. In curves (C) and (E) of all figures the weight of used GO/PAMAM was 0.001 g.

concentrations were estimated as 76%, 79%, 59%, 80%, 45% and 30% of their initial concentrations, respectively.

An increase in the absorbance intensity when the used dyes were adsorbed in the presence of ARS and GO/PAMAM simultaneously, compared to that in the presence of ARS alone, confirmed that due to the complete adsorption of ARS on adsorbent, most dyes molecules remained in the supernatant. Furthermore, some adopted dyes molecules interacted both with surface adsorption sites and adsorbed ARS molecules, peaks of B, C of Figures 14(b)–14(g). It was observed that in the used initial concentrations of ARS and JG, the ARS–JG deposit formed in their mixture was completely dissolved in the presence of GO/PAMAM and the solution turned blue from colorless which was due to complete adsorption of ARS, Figure S5 and peak D of Figure 14(g).

4 Conclusions

The adsorption of ARS on the surface of GO/PAMAM was studied under different temperatures, pHs, ARS initial concentrations, contact times and shaking rates. Adsorption isotherms were analyzed by the ARIAN model and its kinetic curves were investigated by the KASRA model and ISO and intraparticle diffusion equations. Analysis of adsorption isotherms and kinetic curves showed that phenolic –*OH* groups of GO moiety *(Ph)* and $-NH_2$, $-NHR^+_2$ and $-NH^+_3$ groups of PAMAM dendrimer moiety of GO/PAMAM were adsorption sites of the adsorbent. Depending on the solution pH, due to deprotonation, ARS formed three different species as ARS^-, ARS^{2-} and ARS^{3-}. At acidic pHs, ARS^- molecules interacted with *Ph*, $-NH^+_3$ and $-NHR^+_2$ in sequence. The adsorption on the *Ph* and $-NH^+_3$ sites were exothermic and the adsorption on the $-NHR^+_2$ sites was endothermic, respectively.

At pHs of 1, 2 and 3, $q_{e,max}$ of the adsorbent for ARS^- attained to maximum value and were similar together. At pH = 2 and 328 K, $q_{e,max}$ of GO/PAMAM (as a superadsorbent) for the adsorption of ARS^- was 1275.6 mg g^{-1}. This was attributed to the open GO/PAMAM structure after the protonation of all primary and tertiary amine groups of PAMAM dendrimer. Due to the repulsion interaction between these groups, GO/PAMAM structure became very open and resulted in an increase in adsorption capacity of GO/PAMA for ARS. At pH = 2, binding constant values of ARS^- molecules to *Ph* sites were higher than those of $-NH^+_3$ and $-NHR^+_2$ sites of adsorbent. The interaction of ARS^- molecules with *Ph* sites was faster than that of $-NH^+_3$ and $-NHR^+_2$ sites. The adsorption of ARS^- on *Ph* sites was reaction-controlled. The activation energy obtained from its ISO rate constant was 114.5 kJ mol^{-1}. However, the adsorption of ARS^- on the $-NH^+_3$ and $-NHR^+_2$ sites was diffusion-controlled.

The decrease in the pH of solutions from 1 to 0 resulted in a decrease in $q_{e,max}$, which could be owe to fewer available *Ph*, $-NH^+_3$ and $-NHR^+_2$ groups of GO/PAMAM for ARS molecules that was caused by a shrinkage in GO/PAMAM structure and masking some of functional groups of GO/PAMAM. Also, this resulted in a decrease in ISO rate constants with a decrease in pH from 2 to 0. At pH = 5, ARS^- interacted first with *Ph* sites and then with $-NH^+_3$ sites. In continuation, ARS^{2-} interacted with $-NH^+_3$ adsorption sites.

At pHs of 11 and 13, ARS^{3-} molecules at first interacted with $-NH^+_3$ and then $-NH_2$ adsorption sites. At pH of 14, ARS^{3-} molecules interacted with $-NH_2$ adsorption sites only. Different types of ARS molecules in acidic and alkaline media interacted with GO/PAMAM adsorption sites through their sulfonate head.

By using GO/PAMAM, several dyes including MB, AO, Th, PY, MEB and JG were separated from their mixtures with ARS at pH of 2. Our extensive study illustrated that used adsorbent was regenerated completely and efficiently using ethylenediamine at ambient temperature.

Furthermore, GO/PAMAM can be used to selectively remove ARS from dye mixtures at pH of 2. The finding could be beneficial to fabricate photochemical and electrochemical sensors.

5. References

1. M. F. Hamoda, I. Al-Ghusain, N. Z. Al-Mutairi, *Desalination*, **2004**, *164*, 203–211. **DOI:**10.1016/S0011-9164(04)00189-4
2. O. Tunay, E. Erdeml, N. Işık Kabdaşlı, T. Olmez, *Environ. Technol.*, **2008**, *29*, 1045–1051. **DOI:**10.1080/09593330802175823
3. G. Al-Enezi, M. Hamoda, N. Fawzi, *J. Environ. Sci. Health A*, **2004**, *39*, 455–464. **DOI:**10.1081/ESE-120027536
4. R. Hesnawi, K. Dahmani, A. Al–Swayah, S. Mohamed, S. A. Mohammed, *Procedia Eng.*, **2014**, *70*, 810–814. **DOI:**10.1016/j.proeng.2014.02.088
5. S. Palit, *IJCA*, **2012**, *3*, 302–305.
6. E. Nutiu, *Proc. Technol.*, **2015**, *19*, 479–482. **DOI:**10.1016/j.protcy.2015.02.068
7. F. Gorzin, M. M. Bahri Rasht Abadi, *Adsorpt. Sci. Technol.*, **2017**, *36*, 149–169. **DOI:**10.1177/0263617416686976
8. T. Erban, J. Hubert, *J. Insect Sci.*, **2010**, *10*, 1–12. **DOI:**10.1673/031.010.4201
9. J. Šíma, P. Hasal, *Chem. Eng. Trans.*, **2013**, *32*, 79–84.
10. J. H. Miller, J. L. Kotenko, *Stain Technol.*, **1987**, *62*, 237–245. **DOI:**10.3109/10520298709108001
11. M. S. Raghu, K. Basavaiah, K. N. Prashanth, K. B. Vinay, *ISRN Spectroscopy*, **2012**, Article ID 648510. **DOI:**10.5402/2012/648510
12. M. Fayazi, M. Ghanei-Motlagh, M. A. Taher, *Mater. Sci. Semicond. Process.*, **2015**, *40*, 35–43. **DOI:**10.1016/j.mssp.2015.06.044
13. D. Li, Q. Liu, S. Ma, Z. Chang, L. Zhang, *Adsorpt. Sci. Technol.*, **2011**, *29*, 289–300. **DOI:**10.1260/0263-6174.29.3.289
14. L. Fan, Y. Zhang, X. Li, C. Luo, F. Lu, H. Qiu, *Colloids Surf. B: Biointerfaces*, **2012**, *91*, 250–257. **DOI:**10.1016/j.colsurfb.2011.11.014
15. R. K. Gautam, P. K. Gautam, M.C. Chattopadhyaya, S. Banerjee, J. D. Pandey, *Proc. Natl. Acad. Sci., India, Sect. A Phys. Sci.*, **2014**, *84*, 495–504. **DOI:**10.1007/s40010-014-0154-4
16. P. B. Wagh, V. S. Shrivastava, *J. Sci. Res. Rep.*, **2014**, *3*, 2197–2215. **DOI:**10.9734/JSRR/2014/8005
17. F. Fu, G. Ziwei, L. Gao, D. Li, *Ind. Eng. Chem. Res.*, **2011**, *50*, 9712–9717. **DOI:**10.1021/ie200524b
18. S. Gao, W. Zhang, *Adsorpt. Sci. Technol.*, **2019**, *37*, 185–204. **DOI:**10.1177/0263617418819164
19. M. Aissat, S. Hamouda, N. Benhadria, R. Chellali, N. Bettahar, *AIP conference proceedings 1968*, **2018**, ID.020005.
20. H. V. Jadhava, S. M. Khetre, S. R. Bamane, *Der Chemica Sinica*, **2011**, *2*, 68–75.
21. M. Jamshidi, M. Ghaedi, K. Dashtian, S. Hajati, A. Bazrafshan, *RSC Adv.*, **2015**, *5*, 59522–59532. **DOI:**10.1039/C5RA10981G

22. J. Zolgharnein, Z. Choghaei, M. Bagtash, S. Feshki, M. Rastgordani, P. Zolghadrian, *Desalin. Water Treat.*, **2016**, *57*, 27672–27685.
23. O. Ali, S. Mohamed, *Turk. J. Chem.*, **2017**, *41*, 967–986. **DOI:**10.3906/kim-1703-72
24. F. Zhang, B. Wang, S. He, R. Man, *J. Chem. Eng. Data*, **2014**, *59*, 1719–1726. **DOI:**10.1021/je500219e
25. Q. C. Compton, D. A. Dikin, K. W. Putz, L. C. Brinson, S. T. Nguyen, *Adv. Mater.*, **2010**, *22*, 892–896. **DOI:**10.1002/adma.200902069
26. M. Rafi, B. Samiey, C-H Cheng, *Materials*, **2018**, *11*, 496. **DOI:**10.3390/ma11040496
27. K. S. W. Sing, D. H. Everett, R. A. W. Haul, L. Moscou, R. A. Pierotti, J. Rouquerol, T. Siemieniewska, *Pure Appl. Chem.*, **1985**, *57*, 603–619.
28. R. M. Silverstein, G. C. Bassler, T. C. Morrill: Spectrometric Identification of Organic Compounds. Fourth Edition, John Wiley and Sons, New York, 1981.
29. Y. Piao, T. Wu, B. Chen, *Ind. Eng. Chem. Res.*, **2016**, *55*, 6113–6121. **DOI:**10.1021/acs.iecr.6b00947
30. C. Wang, Y. Duan, N. S. Zacharia, B. D. Vogt, *Soft Matter***, 2017, *13*,** 1161–1170. **DOI:**10.1039/C6SM02439D
31. H. Gunzlr, H. U. Gremlich: IR Spectroscopy: An Introduction, Weinheim, Wiley-VCH, 2002.
32. B. Samiey, S. Golestan, *Cent. Eur. J. Chem.*, **2010**, *8*, 361–369. **DOI:**10.2478/s11532-009-0135-7
33. B. Samiey, S. Abdollahi Jonaghani, *J. Pollut. Eff. Cont.*, **2015.** **DOI:**10.4172/2375-4397.1000139
34. I. Langmuir, *J. Am. Chem. Soc.*, **1918**, *40*, 1361–1403. **DOI:**10.1021/ja02242a004
35. M. Boudart, G. Djega-Mariadassou: Kinetics of Heterogeneous Catalytic Reactions. Princeton University Press, New Jersy, 1984. **DOI:**10.1515/9781400853335
36. T. Sekine, T., Nakatani, K., *Langmuir*, **2002**, *18*, 694–697. **DOI:**10.1021/la0110500
37. B. Samiey, A. Dadkhah Tehrani, *JCCS*, **2015**, *62*, 149–162. **DOI:**10.1002/jccs.201400093
38. N. Safar Beyranvand, B. Samiey, A. Dadkhah Tehrani, *Acta Chim. Slov.*, **2019**, *66*, 443–454. **DOI:**10.17344/acsi.2018.4920
39. J. Ghasemi, S. Lotfi, M. Safaeian, A. Niazi, M. M. Ardakani, M. Noroozi, *J. Chem. Eng. Data.*, **2006**, *51*, 1530–1535. **DOI:**10.1021/je050535d
40. J. Ghasemi, A. Niazi, G. Westman, M. Kubista, *Talanta*, **2004**, *62*, 835–841. **DOI:**10.1016/j.talanta.2003.10.003
41. A. Córdoba, I. Magario, M. L. Ferreira, *J. Mol. Catal. A-Chem.*, **2012**, *355*, 44–60. **DOI:**10.1016/j.molcata.2011.12.011
42. P. K. Maiti, T. Çağin, S-T Lin, W. A. Goddard, *Macromolecules*, **2005**, *38*, 979–991. **DOI:**10.1021/ma049168l
43. P. Nuengmatcha, R. Mahachai, S. Chanthai, *Orient. J. Chem.*, **2016**, *32*, 1399–1410. **DOI:**10.13005/ojc/320314
44. Y. Guo, J. Deng, J. Zhu, C. Zhou, X. Zhou, R. Bai, *RSC Advances*, **2016**, *6*, 39762–39773. **DOI:**10.1039/C6RA03423C
45. R. W. Sabins: Handbook of Biological Dyes and Stains: Synthesis and Industrial Applications, John Wiley & Sons, Inc., New Jersey, 2010.
46. M. I. Chaudhari, S. A. Holleran, H. S. Ashbaugh, L. R. Pratt, *PNAS*, **2013**, *110*, 20557–20562. **DOI:**10.1073/pnas.1312458110
47. S. Lüdemann, R. Abseher, H. Schreiber, O. Steinhauser, *J. Am. Chem. Soc.*, **1997**, *119*, 4206–4213. **DOI:**10.1021/ja953439d
48. D. W. Kimmel, G. LeBlanc**,** M. E. Meschievitz**,** D. E. Cliffel, *Anal. Chem.*, **2012**, *842*, 685–707. **DOI:**10.1021/ac202878q
49. F. Li, J. Peng, Q. Zheng, X. Guo, H. Tang, S. Yao, *Anal. Chem.*, **2015**, *879*, 4806–4813.
50. Z. Wang, N. Zhong, M. Chen, H. Chang, D. Zhong, Y. Wu, H. Liu, X. Xin, M. Zhao, B. Tang, T. Song, S. Shi, *Applied Optics*, **2019**, *58*, 2091–2099. **DOI:**10.1364/AO.58.002091

Povzetek

Preučevana je adsorpcija alizarin rdeče S (ARS) na grafen oksid/poli(amidoamin) (GO/PAMAM) glede na različne začetne koncentracije ARS, temperaturo, pH vrednosti, hitrost mešanja in kontaktni čas. Adsorpcijska mesta GO/PAMAM so bile fenolne skupine –*OH* (*Ph*) GO in aminske skupine ($-NH_2$, $-NH^+_3$ in $-NHR^+_2$) PAMAM dendrimernih enot GO/PAMAM. Pri pH vrednosti 2 in temperaturi 318K je bila dosežena maksimalna kapaciteta ($q_{e,max}$) adsorbenta, ki je znašala 1275.2 mg g^{-1} in predstavlja eno najvišjih kapacitet opisanih v literaturi. Zato lahko smatramo, da deluje GO/PAMAM kot superadsorbent za ARS. V začetni fazi je adsorpcija kontrolirana z reakcijo (E_a = 114.5 kJ mol^{-1}) in se ARS^- molekule adsorbirajo na *Ph* mesta. Kasnejša adsorpcija na preostala adsorpcijska mesta pa je difuzijsko omejena. V bazičnem okolju smo identificirali dve drugi obliki ARS molekul, ki so se adsorbirale na *Ph* in $-NH^+_3$mesta. Nadaljnje povečevanje bazičnosti raztopine se je odrazilo v nižanju števila adsorpcijskih mest in posledično nižanju adsorpcijske kapacitete ($q_{e,max}$). Poleg tega smo pri pH vrednosti 2 lahko s pomočjo GO/PAMAM ločili ARS molekule od molekul metilensko modrega, (MB), tionina (Th), pironina Y (PY), akridin oranžnega (AO), metil modrega (MEB) in janus zelenega (JG).